Low Limit of Detection Gas Density Sensing With a Digitally PI-Controlled Microcantilever

João Mouro, Paolo Paoletti, Marco Sartore, and Bruno Tiribilli

***Abstract*—This work describes a new platform for sensing mass or rheological properties of gases with unprecedented responsivity and limits of detection. The system consists of a microcantilever working in a phase-locked loop (PLL) with an imposed phase between its excitation and deflection signals. The optically detected cantilever deflection is demodulated against digitally synthetized reference signals, and the quadrature component (*Q*-signal) is used as the error parameter in a PI controller, which continuously tracks the oscillation frequency. The direct digital synthesis of the reference and actuation signals allows low-noise and fast-transient responses of the sensor for real-time detection of minute changes of any environmental parameter. A general analytical model is derived, used to understand the dynamical response of the platform, and validated against experiments using different gases and pressures. In particular, the responsivity of the sensor to density variations of the fluids and the stability of its frequency response are studied and measured. It is shown that the responsivity and the achieved limits of detection depend on the chosen phase imposed in the loop. A limit of detection for density variations of 3.5×10^{-4} kg/m^3 in air is measured, in agreement with the theoretical predictions, and one to two orders of magnitude lower than any reported value achieved with the same type of physical uncoated resonant sensors.**

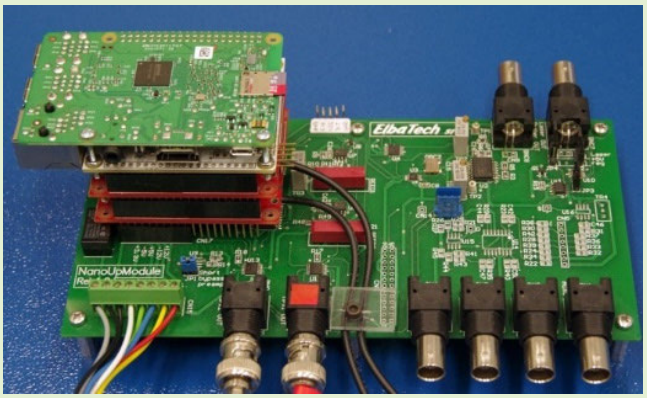

***Index Terms*— Density sensing, limit of detection, microcantilever, responsivity.**

I. Introduction

DETECTING and discriminating the presence of different gas molecules is crucial in environmental monitoring, industrial and chemical control, and medical applications. Solid-state miniaturized devices have been proposed in the last decade for different gas sensing applications due to their high responsivity, fast response time, and low limits of detection.

One common gas sensing method is based on the chemoresistive effect. The electrical conductivity of some materials with very stable electronic properties can be strongly influenced by the adsorption of extrinsic molecules, which can act as surface donors or acceptors of electrons. The detection of molecules of NO_2 adsorbed on graphene [1], [2], [3], SnO_2 nanowires [4], or single-walled carbon nanotubes (SWCNTs) [5] is the examples of this detection method. Recently, a new customizable, low-power, and wireless platform has been developed to address resistive nanosensors [6].

Another possible sensing strategy consists of using suspended resonators, whose resonance frequency changes when specific gas molecules attach [7]. For example, H_2 adsorption on Pd-coated clamped bridges induces an axial stress responsible for decreasing the resonance frequency of the device [8]. On the other hand, the mass of functionalized resonators increases by the adsorption of CO_2 by zeolitic imidazolate framework (ZIF) [9], CO by ZnO [10], or ethanol vapors by a phthalocyanine copper layer [11]. The detection of shifts in the resonance frequency across several simultaneous resonant modes was reported in metal–oxide framework (MOF)-coated microbeams [12], [13]. More recently, nanostructured microcantilevers have also been proposed for sensing molecules in the vapor phase, showing improved selectivity and responsivity. For example, a 3-D framework of ZnO nanorods on Si-nanopillars was functionalized with a self-assembled monolayer for interacting with NO_2 [14]. Also,

Manuscript received 19 December 2022; revised 13 February 2023; accepted 24 February 2023. Date of publication 8 March 2023; date of current version 14 April 2023. This work was supported by the European Union's Horizon 2020 Research and Innovation Program under Marie Skłodowska-Curie Grant 842147. The associate editor coordinating the review of this article and approving it for publication was Prof. Stefan J. Rupitsch. *(Corresponding author: João Mouro.)*

João Mouro and Bruno Tiribilli are with the Institute for Complex Systems of the National Research Council (CNR-ISC), 50019 Florence, Italy (e-mail: joao.mouro@isc.cnr.it).

Paolo Paoletti is with the School of Engineering, University of Liverpool, L69 3GH Liverpool, U.K. (e-mail: paoletti@liverpool.ac.uk).

Marco Sartore is with ElbaTech Srl, 57030 Marciana, Livorno, Italy (e-mail: sartore@elbatech.com).

Digital Object Identifier 10.1109/JSEN.2023.3251865

3-D arrays of nanorods of TiO_2 and MnO_2 were synthetized on a commercial silicon cantilever and used to detect chemical warfare agents, such as dimethyl methylphosphonate [15].

Common to all the abovementioned examples is the chemical functionalization of the sensors. Chemical sensors are attractive due to their very high selectivity and sensitivity, allowing the detection of some gases in concentrations of the order of the parts per billion (ppb) [6], [16]. However, these also require difficult chemical or microfabrication steps for functionalization to a specific target, are prone to reliability and stability issues, are limited by the adsorption and diffusion processes at the surface, have slow response times, and require frequent calibration and cleaning steps [17], [18].

To circumvent these problems, physical gas sensors can be used. These are uncoated devices, capable of detecting a physical property of the environment in which they are immersed, and relate it with a certain gas or a composition of gases. A common sensing strategy relies on microthermal conductivity detectors. A heated device will reach a temperature, which depends on the thermal conductivity of the gaseous atmosphere surrounding the sensor. Steady-state [19] or transient state [20], [21] sensors exploiting this phenomenon have been proposed. The temperature of the microbeam can in addition be used to control the axial stress and resonance frequency of the beams near the buckling bifurcation point [22].

A different strategy consists of using uncoated resonators. These are highly responsive to changes in the surrounding environment and can promptly detect changes in physical properties of fluids. In fact, the dynamical response of microcantilevers strongly depends on the density and viscosity of the media, and shifts in quality factor [23] and/or resonance frequency [17], [24], [25], [26] have been used to discriminate the presence of gases [18]. These works are based on the interaction between a viscous fluid and a microcantilever, derived analytically by Sader [27], Van Eysden and Sader [28], and Maali et al. [29].

Regardless of the sensing principle, current works aim at simplifying the hardware setup, using digital electronics for maximum freedom of operations and at improving the versatility, responsivities, and limits of detection of the sensor [6]. In this work, we report a new sensing platform that uses an uncoated microcantilever as a physical sensor for real-time sensing, with unprecedented responsivity and limit of detection. In particular, we study the case of mass density sensing and derive and validate a general model and method to study the dynamical response of the system.

II. Methods

A. Proposed Platform

The proposed platform consists of a microcantilever self-excited in a phase-locked loop (PLL), comprising optomechanical and electronics modules. The optomechanical module, detailed in Fig. 1(A), is used to excite the microcantilever, oscillating in a viscous fluid within a closed cell, and optically detect its deflection with a laser reflected to a four-quadrant detector. The electronics module, detailed in Fig. 1(B), contains three direct digital synthesizers (DDDs),

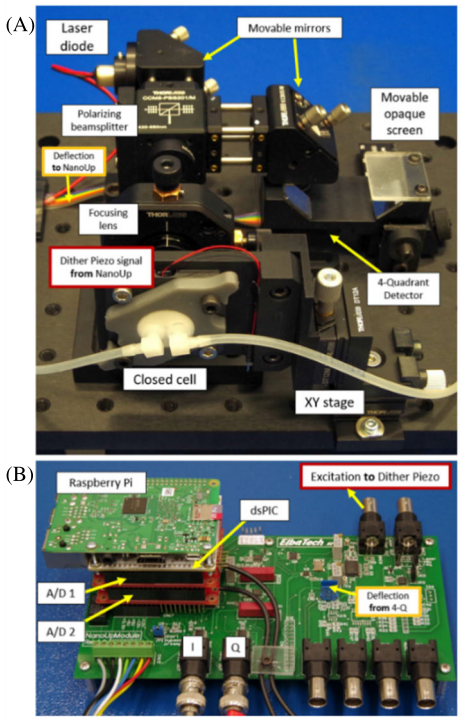

Fig. 1. Proposed platform consisting of (A) optomechanical module and (B) electronics module.

two low-pass filters (LPs), two analog-to-digital converters (A/Ds), a dsPIC microcontroller, and a Raspberry Pi and is used to analyze the deflection signal of the cantilever and generate the excitation voltage sent to the excitation piezo in real time. Fig. 2(A) shows a schematic of the electrical signals throughout the platform, whereas Fig. 2(B) shows a high-level block diagram. The green dashed line and block [in Fig. 2(A) and (B)] represent the optomechanical unit, while the orange dashed line and blocks represent the electronics module. Red arrows indicate the digital signals.

In general, the deflection signal coming from the optomechanical unit is fed to the electronics unit, where it is demodulated by two reference direct-digital-synthesis signals [DDS-sine and DDS-cosine, Fig. 2(A)]. The in-phase and quadrature components, I and Q, respectively, are filtered and converted to digital [A/D1 and A/D2, Figs. 1(B) and 2(A)]. The Q-signal is fed to the programmed dsPIC and used as the error parameter in a PI controller, which continuously adjusts the frequency ω of the synthetized DDS reference signals and yet another DDS signal, which is used to excite the microcantilever [DDS-dither, Fig. 2(A)]. A phase difference ϕ, chosen by the user, is imposed between the reference and the dither excitation synthetized signals.

The excitation signal (DDS-dither) is finally fed back to the dither piezo in the optomechanical unit to excite the microcantilever. The Raspberry Pi indicated in Figs. 1(B) and 2(B) is used to interface the dsPIC microcontroller with the graphical user interface (GUI) software, transmitting data and commands during experiments. A more detailed description of the platform can be found in Appendix A.

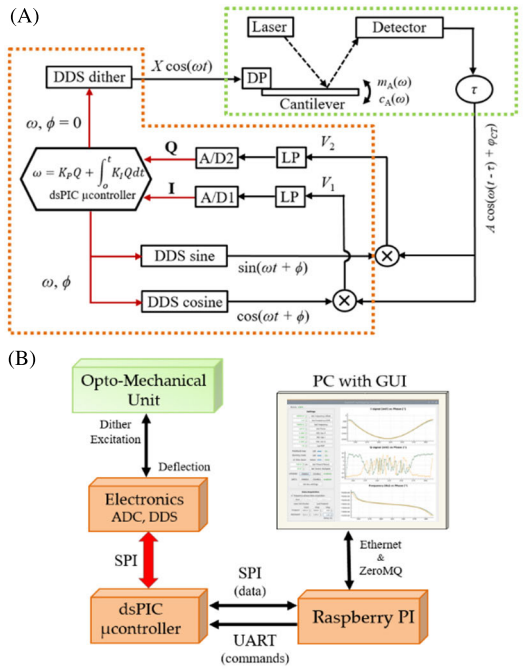

Fig. 2. Complete schematic of the developed platform. (A) Electrical signals. (B) Block diagram. A complete description of the platform can be found in Appendix A.

B. Analytical Model

This system works as a PLL, with an imposed fixed phase ϕ between the excitation signal and the cantilever deflection. Any environmental change can then be detected by measuring the frequency and/or the amplitude of oscillation in real time. The microcantilever is modeled as a damped harmonic oscillator, including the added mass and damping terms caused by the interaction with the surrounding viscous medium [27], [29]. The oscillation frequency of the closed feedback loop [see Fig. 2(A)] imposed by the PI controller, ω, is obtained by considering the steady state of the system (quadrature component $Q = 0$). The oscillation frequency is a complex nonlinear function of the density and viscosity of the surrounding medium, microcantilever geometry, and imposed phase in the system ϕ and can be calculated by solving the following expression:

$$-\omega\tau + \operatorname{atan}\left(-\frac{\omega\,(c_0 + c_A)}{m_0\omega_0^2 - (m_0 + m_A)\,\omega^2}\right) - \phi = -\left(\frac{\pi}{2} + n\pi\right) \quad (1)$$

with $n = 0, 1, 2, \ldots$, defining the branch, where the response of the system gets locked, τ the total time delay of the signals around the loop (mostly due to the propagation of the acoustic waves from the excitation dither piezo to the cantilever through the cantilever holder), and m_A and c_A are the added mass and damping coefficients, respectively, due to the presence of the fluid, given by

$$m_A = \frac{\pi}{4}\rho L W^2\left(a_1 + \frac{a_2}{W}\sqrt{\frac{2\eta}{\rho\omega}}\right) \quad (2)$$

$$c_A = \frac{\pi}{4}\rho L W^2\omega\left(\frac{b_1}{W}\sqrt{\frac{2\eta}{\rho\omega}} + \frac{b_2}{W^2}\frac{2\eta}{\rho\omega}\right) \quad (3)$$

where ρ and η are the density and viscosity of the surrounding fluid, respectively, $a_1 = 1.0553$, $a_2 = 3.7997$, $b_1 = 3.8018$, and $b_2 = 2.7364$ are the constants to describe the hydrodynamic function [29], L and W are the length and width of the cantilever, respectively, and ω_0, m_0, and c_0 are its natural frequency, mass, and intrinsic damping, respectively. Equation (1) is solved numerically to extract the oscillation frequency of the system ω as a function of the rheological parameters of the media.

The frequency of the oscillation ω calculated with (1) is then used to determine the I-signal of the system using

$$I = \frac{A}{2}\sin\left(\frac{\pi}{2} + n\pi\right) = \begin{cases} \frac{A}{2}, & \text{for } n = 0, 2, 4, \ldots \\ -\frac{A}{2}, & \text{for } n = 1, 3, 5, \ldots \end{cases} \quad (4)$$

where A is the amplitude of oscillation, given by

$$A = \left[\left(\frac{m_0\omega_0^2}{(m_0 + m_A)} - \omega^2\right)^2 + \left(\frac{\omega\,(c_0 + c_A)}{(m_0 + m_A)}\right)^2\right]^{-\frac{1}{2}}. \quad (5)$$

These expressions are derived in detail in previous works [30], [31], in which a very similar system was used to measure the viscosity and viscoelastic properties of liquids.

III. Results

A. Phase Characterization of Different Gases

A doped single crystal silicon cantilever ACST-TL from AppNano was used in the experiments. This has nominal dimensions of $L = 160\ \mu$m, $W = 28\ \mu$m, and $T = 3.0\ \mu$m and a resonance frequency and quality factor in air of $f_0 = 164.36$ kHz and $Q_0 = 250$.

The first characterization of the system consisted of sweeping the imposed phase ϕ in the interval $[0, -2\pi]$, while detecting the frequency and amplitude of oscillation of the closed-loop under stable environmental conditions. Experimental and modeled oscillation frequencies and I-signal [or amplitude, see (4)] are shown in Fig. 3 as a function of the imposed phase ϕ.

Fig. 3(A) shows the case of measurements in air at atmospheric pressure. Two distinct oscillation branches are observed, corresponding to the repeated periodic phase response of the microcantilever [32], over the complete 2π cycle of imposed phase ϕ. A slope is observed at the limits of the branches, due to the delay of the loop, $\tau = 10.65\ \mu$s [33]. Equation (1) models analytically each different branch by admitting a different value of n. Experimentally, these different branches are observed by using positive or negative gains of the PI controller. Three distinct imposed phase points are highlighted and will be further discussed in Figs. 4, 5 and 6.

Fig. 3(B) shows the frequency and I-signal response of the microcantilever when immersed in different gases at atmospheric pressure and temperature. Experimental results (for He and N_2 gases) and simulations using (1) and (4) (for six different gases) are shown for the first branch ($n = 4$). Each

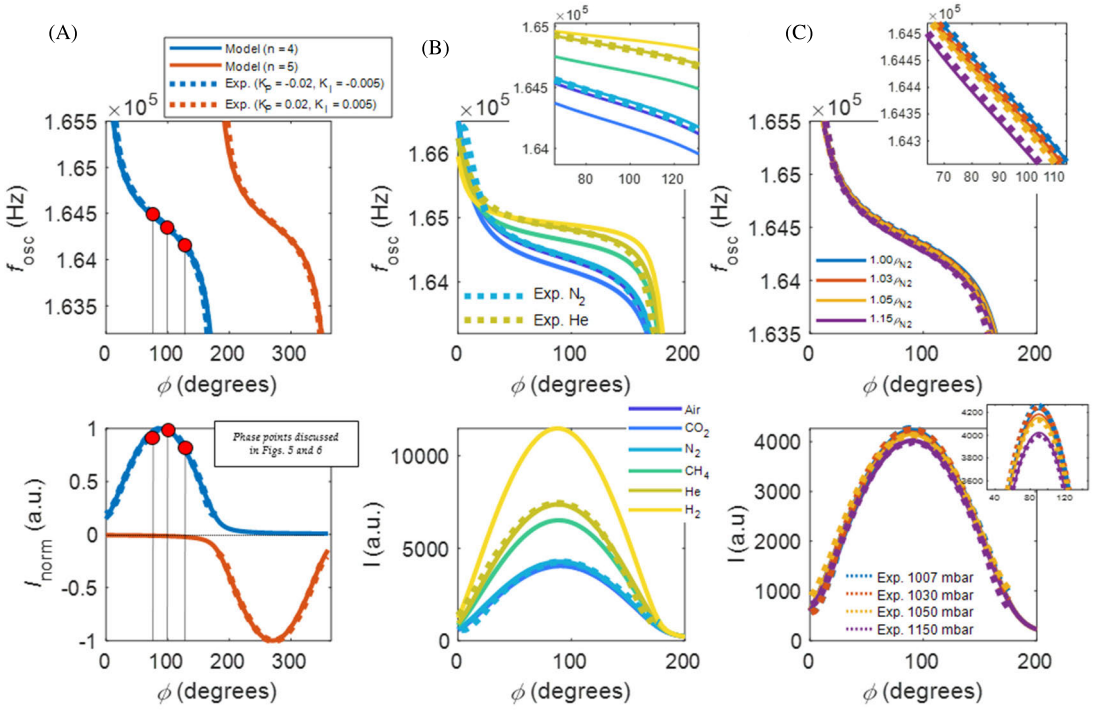

Fig. 3. Measured (dashed lines) and modeled (solid lines) oscillation frequencies (top) and amplitudes (bottom), as a function of the imposed phase ϕ. (A) Air at atmospheric pressure. Two periodic branches are shown, corresponding to different n in the model of (1) and different gains of the PI controller in experiments. (B) Different gases at atmospheric pressure. (C) N_2 at different pressures (densities). Insets show the details of the data.

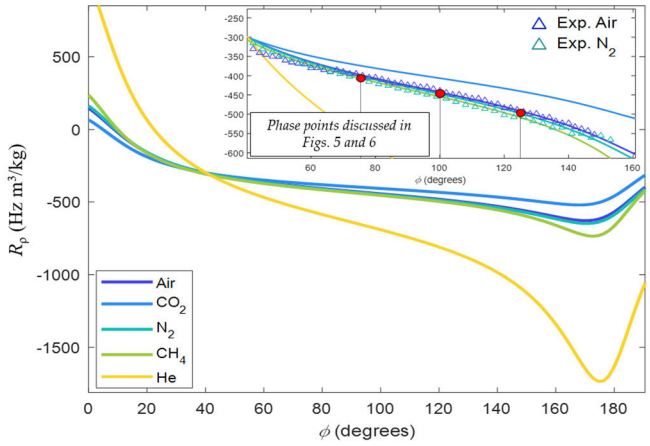

Fig. 4. Modeled sensitivities (solid lines) for different gases, as a function of the imposed phase ϕ in the system. Inset: experimental data (colored symbols) obtained from the pressure curves for air and N_2. Three phase points are highlighted for the ensuing discussion.

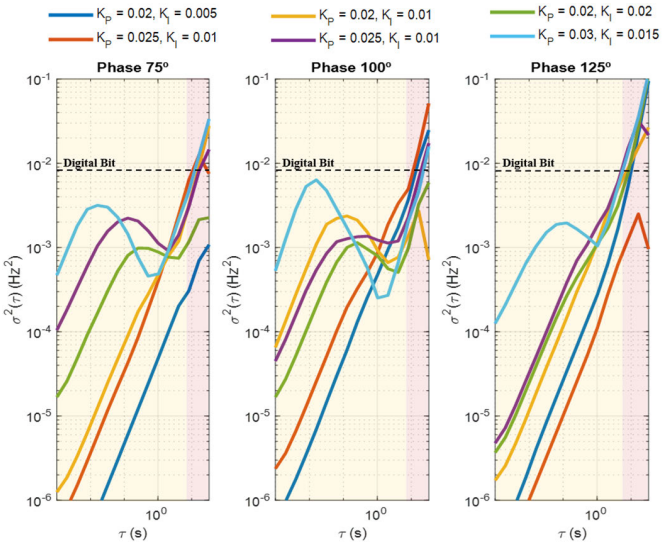

Fig. 5. Allan variation for different controller conditions and imposed phases. Red areas indicate regions, where the frequency drift prevents detecting the smallest digital frequency bit of the platform, or δf_s.

gas presents a different signature response, resulting from the different densities and viscosities that alter the added mass and damping coefficients given by (2) and (3).

Finally, Fig. 3(C) shows the response of the cantilever when immersed in N_2 at different pressures and room temperature. Experimentally, the pressure in the cell was increased from the atmospheric pressure of 1007–1150 mbar. A proportional increase in the value of density (from 0% to 15%) was considered in (1) and (4) of the model. Increasing the pressure in the closed cell (or, equivalently, the density of the fluid) decreases both the oscillation frequency and amplitude due to the increased added mass and damping coefficients.

The developed analytical model captures the response of the microcantilever in different conditions and can therefore be used to predict the responsivity of the sensor. A particular case of density variations will be studied next to validate the performance of the platform.

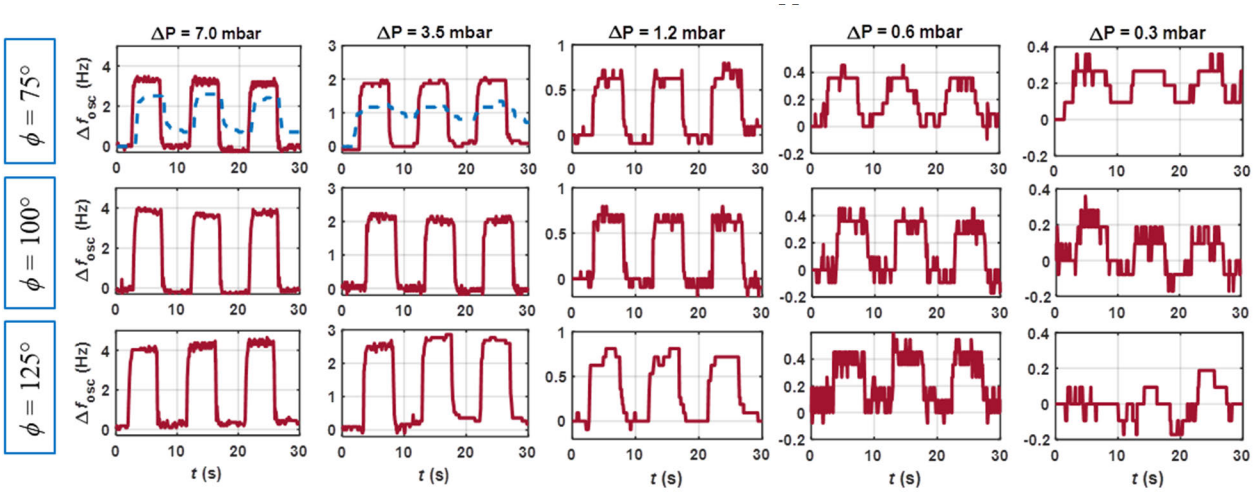

Fig. 6. Pressure cycles for fixed imposed phases ϕ, using well-tuned controller ($K_P = 0.02$ and $K_I = 0.02$). The blue dashed line on the top left corresponds to a poorly tuned controller ($K_P = 0.02$ and $K_I = 0.005$) (dark blue line in Fig. 5), showing slow transient response and offset error.

B. Responsivity to Density Variations

The responsivity of the sensor to density variations is defined as the change of oscillation frequency in response to changes in the density of the fluid, or $R_\rho = (\partial f/\partial \rho)$. Equation (1) is a highly nonlinear function, which prevents a simple analytical estimation of the responsivity. However, in first approximation, it can be assumed that the dependence between the oscillation frequency of the system, f, and the density of the fluid, ρ, is linear, and

$$R_\rho\,(\phi, \eta, \rho, L, W, \tau, m_0, c_0, \ldots) = \frac{\partial f}{\partial \rho} \approx \left(\frac{f_2 - f_1}{\rho_2 - \rho_1}\right) \quad (6)$$

in units of Hz m^3/kg. The point 1 in (6) represents the initial working point (with an oscillation frequency of f_1 at a density ρ_1), which is then perturbed to the new working point 2 by a small change of density (with ρ_2 causing an oscillation at f_2). Fig. 4 shows the modeled responsivity of the sensor to density variations of different gases as a function of the imposed phase ϕ, calculated with (1) and (6) and considering $\rho_1 = 1.00\rho$ and $\rho_2 = 1.15\rho$ [corresponding to the same experimental 15% pressure variation shown in Fig. 3(C)]. It can be observed that the responsivity to density variations depends on the imposed phase ϕ on the system, independent of the gas considered. Therefore, the desired response of the system should be controlled by selecting optimal values of the imposed phase ϕ for obtaining higher responsivities and lower limits of detection. In particular, using higher values of imposed phase (or, equivalently, working at below the natural resonance frequency, see Fig. 3) is advantageous for sensing applications, since considering, for example, the case of air (dark blue line), at $\phi = 125°$, $R_\rho \sim 470$ Hz·m^3/kg, while for $\phi = 75°$, $R_\rho \sim 400$ Hz·m^3/kg.

The pressure variation in the experiments is proportional to density variations of the gases in the model. One can use the ideal gas law, $P = \rho(RT/MM)$, with MM the molar mass of the gas, to convert pressure to density, as in

$$R_\rho = \frac{\partial f}{\partial \rho} = \frac{\partial f}{\partial P}\frac{\partial P}{\partial \rho} = \frac{\partial f}{\partial P}\frac{RT}{MM} = \frac{0.08314\ T}{MM}\left(\frac{f_2 - f_1}{P_2 - P_1}\right) \quad (7)$$

with $R = 0.08314$ (dm^3·bar)/(K·mol), T in K, MM in g/mol, f in Hz, and P in bar. As defined in (7), R_ρ has the units of Hz·dm^3/g = Hz·m^3/kg, which are the same units of (6). Equation (7) makes it possible to calculate the experimental responsivity values for air and N_2 from the experimental pressure curves [see Fig. 3(C)], which is shown in the inset of Fig. 4. As presented in (6), the responsivity to density is also a function of the individual geometry of the resonator and rheological properties of the surrounding fluid. This particular sensor shows a responsivity of ~470 Hz·m^3/kg for Air and N_2 and ~800 Hz·m^3/kg for He and H_2, considering an imposed phase of $\phi = 130°$. According to [15], the responsivity increases for wider and thinner sensors.

The selection of the operating value of phase ϕ cannot be limited to the desired responsivity but must also take in account the amplitude of oscillation (I-signal). At low amplitudes, the transient response of the system is slower and noisier—the value of Q, used as the error parameter in the PI controller, depends on the amplitude of the resonator I—and therefore, too far for the resonance, the amplitude may not be proper for real-time sensing.

C. Noise and Minimum Frequency Shift

The frequency response of any real case resonator shows fluctuations due to the noise present in the mechanical and detection systems, electronic components, and surrounding environment. These fluctuations can limit the frequency detection when measuring shifts due to environmental changes, such as those induced by gas density variations. The minimum detectable frequency shift in the system presented in this work is, in theory, the smallest step of frequency generated by the digital synthesizers (hereafter defined as δf_s), or $\delta f_s = 0.0894$ Hz (see Section IV). Therefore, the frequency stability of the system was studied to understand if this tiny frequency shift could indeed be detected, instead of being buried in the intrinsic frequency fluctuations of the platform.

The frequency stability of an oscillator is typically quantified in the time domain by the Allan variation. This quantity is the mean of the squared differences between consecutive

TABLE I
FREQUENCY SHIFTS, RESPONSIVITY, AND LIMIT OF DETECTION

			∂f (Hz)		
∂P (mbar)	$\partial\rho$ (kg/m^3)	$\partial\rho/\rho$ (%)	$\phi = 75°$	$\phi = 100°$	$\phi = 125°$
$\mathbf{7.0 \pm 0.1}$	8.4×10^{-3}	0.65	3.31 ± 0.14	4.02 ± 0.12	4.07 ± 0.13
$\mathbf{3.5 \pm 0.1}$	4.2×10^{-3}	0.33	1.88 ± 0.11	2.11 ± 0.11	2.36 ± 0.08
$\mathbf{1.2 \pm 0.1}$	1.4×10^{-3}	0.09	0.61 ± 0.07	0.71 ± 0.10	0.72 ± 0.06
$\mathbf{0.6 \pm 0.1}$	$\mathbf{7.0 \times 10^{-4}}$	**0.045**	$\mathbf{0.28 \pm 0.07}$	$\mathbf{0.36 \pm 0.11}$	$\mathbf{0.32 \pm 0.11}$
$\mathbf{0.3 \pm 0.1}$	3.5×10^{-4}	0.0225	0.15 ± 0.08	0.20 ± 0.09	-

frequency measurements taken in nonoverlapping time windows of duration τ, as in [32]

$$\sigma_y^2(\tau) = \frac{1}{2(M-1)} \sum_{i=1}^{M-1} (f_{i+1} - f_i)^2 \tag{8}$$

in units of Hz^2, with M is the total number of frequency measurements and f_i the ith frequency measurement (averaged in the time window with duration τ).

Fig. 5 shows the results of measuring the Allan variation of the resonator for different controller conditions, at the three different imposed phases highlighted previously ($\phi = 75°$, 100°, and 125°). These measurements consisted of fixing the phase value, choosing the proportional and integral gains of the controller, letting the system stabilize, and acquiring the oscillation frequency for 100 s at 1000 sample/s.

It can be observed that, regardless of the phase value and controller conditions, for integration times longer than 6–7 s, the frequency drifts away due to temperature fluctuations, laser instabilities, or any other environmental variations (red areas in Fig. 5). This drift is around 0.1 Hz^2 (0.32 Hz), after 90 s, and, therefore, reliable detection of $\delta f_s = 0.0894$ Hz at this time scale is prevented.

Conversely, for integration times shorter than 7 s, it is possible to detect $\delta f_s = 0.0894$ Hz for each chosen phase value (yellow areas in Fig. 5). However, it is still necessary to consider the controller conditions in this region: poorly tuned controllers, such as those with low proportional/integral gains (dark blue, orange, and yellow lines in Fig. 5) show very little noise and frequency fluctuations, but mostly because these are unable to respond to any external stimulus, which cause slower transient responses and often an offset error (shown in Fig. 6). Properly tuned controllers (purple and green lines in Fig. 5) show stronger frequency fluctuations but are also more responsive to an external stimulus. If the gains are too high (light blue line), an oscillatory response can arise and the noise in the short integration times will be bigger than δf_s. Adequate methods and strategies to tune controllers in PLLs to achieve fast transients and noiseless responses are an active branch of research [34], [35], [36]. The slightly different responses of the system for different phases shown in Fig. 5 are caused by the amplitudes of the cantilever deflection in these specific working points. Fig. 3(A) confirms that the amplitude of deflection is larger near the resonance ($\phi = 100°$), then at higher frequencies ($\phi = 75°$) and finally at lower frequencies ($\phi = 125°$). The continuously updated value of the error parameter Q depends on the amplitude of deflection I and, therefore, also impacts the frequency noise of the system.

Optimal experimental operating phase and controller conditions allow to detect frequency shifts equal to $\delta f_s = 0.0894$ Hz in processes occurring in the subsecond to 5-s period. This will be demonstrated in the next section.

D. Limit of Detection for Density Variations

A set of validation experiments are used to assess the limit of detection of the proposed system. These consist of fixing the phase ($\phi = 75°$, 100°, and 125°) and the controller conditions ($K_P = 0.02$ and $K_I = 0.02$—green line of Fig. 5) and cycling the pressure in the cell filled with air, while measuring the oscillation frequency of the system.

Different variations of pressure were tested, until the induced shifts in oscillation frequencies approached δf_s. The results are shown in Fig. 6 and compiled in Table I in Appendix B.

As seen in Fig. 6, the same applied pressure change induces a larger frequency shift when the phase increases from $\phi = 75°$ to 125°, in agreement with the dependence of the responsivity to density on the imposed phase shown in Fig. 4. Reducing the pressure variation causes a proportional reduction on the shifts in oscillation frequency, regardless of the imposed phase. The 0.6-mbar pressure variation of corresponding to a density variation of

$$\Delta\rho = \frac{\Delta P M M}{RT} = \frac{0.6\times10^{-3}29}{0.08314293} = 7.0\times10^{-4}\ \text{kg/m}^3 \tag{9}$$

allows to still clearly detect 3–4 bits of frequency (3–4 δf_s) or around 0.35 Hz. In fact, jumps of $2\delta f_s$ can still be observed (right panels) for a pressure variation of 0.3 mbar (or $\Delta\rho = 3.5\times10^{-4}$ kg/m^3). In this case, the jumps induced by the noise are comparable to those induced by the pressure variations. The limit of detection of the proposed platform can be calculated by the definition [28]

$$\text{LoD}_\rho = 3\frac{\delta f_{\min}}{R_\rho} \tag{10}$$

in units of kg/m^3, where, as shown, $\delta f_{\min} = \delta f_s = 0.0894$ Hz, and R_ρ is the responsivity of the system to density variations as presented in Fig. 4. Equation (10) assumes that a three-standard deviation of frequency change can be understood as a measurement instead of noise. By substituting in (10) the

TABLE II
COMPARISON OF RESONANT DENSITY SENSORS

	Tétin (2010) [24]	**Rosario (2014) [25]**	**Badarlis (2015) [26]**	**Boudjiet (2015) [17]**	**This work**
Measurement	Electromagnetic actuation Piezoresistive sensing Measure binary mixtures of He/ N_2 and CO_2/N_2	Piezoelectric actuation Impedance sensing Measure sequential flows of He-Ar-N_2	Electromagnetic actuation Piezoresistive sensing Measure 6 different gases and 16 binary mixtures	Electromagnetic actuation Piezoresistive sensing Measure binary mixture of H_2/N_2	Piezoelectric actuation Optical sensing Measure Air, N_2 and He
System	Open-loop	Open-loop	Open-loop	Open-loop	Closed-loop
Cantilever	mm-sized cantilevers 5 different geometries f_R= 4-50 kHz	mm-sized cantilevers 4 different geometries f_R= 15-50 kHz	mm-sized cantilever 1 single geometry f_R= 34 kHz	U and T-shaped mm-sized cantilevers Different geometries f_R= 2-40 kHz	µm-sized cantilever 1 single geometry f_R= 164.4 kHz
Responsivity Method	Hydrodynamic function and Euler-Bernoulli beam equation $\frac{\delta f_R}{f_R} = -\frac{\pi a_1 W}{8T}\frac{\delta\rho}{\rho}$	Linear fit between the frequency and density variations	Fit of Hydrodynamic function into the open loop transfer function of the damped harmonic oscillator model	Hydrodynamic function and Euler-Bernoulli beam equation $\frac{\delta f_R}{\delta\rho} = -\frac{a_1 W}{\rho L^2}\frac{1.875^2}{16}\sqrt{\frac{E}{12\rho_c}}$	Linearization of frequency solution around the working density for different imposed phases
Measured Responsivity R_ρ (Hz m³/kg)	-	20.4	240	40-230	(For $\phi = 130°$) ~ 470 (Air, N_2)
Measured LoD ($\delta\rho$) (kg/m³)	0.03 (CO_2 in H_2) 0.02 (He in H_2)	0.49 (Ar in N_2)	--	0.002 (H_2 in N_2)	0.00035 (Air)
Theoretical LoD ($\delta\rho$) (mg/m³)	Calculated with $LoD_\rho = 3\frac{\delta f_{min}}{R_\rho}$ Assuming $\delta f_{min} = 1$ mHz Optimized geometry 550 (CO_2 in H_2) 33 (He in H_2)	Calculated with $LoD_\rho = 3\frac{\delta f_{min}}{R_\rho}$ Assuming $\delta f_{min} = 0.6$ Hz 88000 (Ar in N_2)	--	Calculated with $LoD_\rho = \frac{3}{SNR}$ 110 (H_2 in N_2)	Calculated with $LoD_\rho = 3\frac{\delta f_{min}}{R_\rho}$ Assuming $\delta f_{min} = \delta f_s = 1$ mHz (digital bit) Optimized geometry to double responsivity 5 (CO_2) 2.2 (He) 2.0 (H_2)

corresponding values, one can expect a limit of detection (with this particular geometry of cantilever and a properly chosen imposed phase ϕ) of around 7.0×10^{-4} kg/m^3 in air or N_2, or 4.0×10^{-4} kg/m^3 in He. The theoretical value calculated with (10) is identical to the values experimentally measured in air in the experiments shown in Fig. 6 [and calculated with (9)] and in Table I in Appendix C.

IV. DISCUSSION

In this work, we present a real-time sensing platform which uses a resonant uncoated microcantilever for detecting gas density changes with the best limit of detection reported to date. We present a sensing platform for real-time measurements of mass or rheological properties with high responsivity and low limits of detection. A general analytical model is used to capture the dynamical response of the uncoated resonant microcantilever and its response to variations of the environmental properties. This model is validated by performing experiments using different gases and pressures. In particular, we highlight the operation of the system as a gas density sensor and show the best limit of detection of gas density variation reported to date with this type of sensors. Table II in Appendix C shows a comparison of the state-of-the-art of physical resonant gas density sensors reported in the last years, discussing the methodology, responsivities and limits of detection of each one, and highlighting the advantages of this platform proposed here. Our shorter cantilever has a higher resonance frequency ($\sim 4x$, third row) and a higher responsivity ($\sim 2x$, fifth row). However, the reported LoD (sixth row) does not scale proportionally and is one to two orders of magnitude lower. This is mostly due to the ability of detecting the tiniest frequency shift induced by density variations with the low-noise electronics and making use of the improved responsivities at high imposed phases.

Improving the limits of detection of this system is still possible by increasing the responsivity of the sensor or by decreasing the minimum detectable step in frequency, δf_s. The first can be achieved by optimizing the geometry of the sensor, using, for example, a higher width-to-thickness ratio. The latter can be achieved by increasing the resolution frequency of the synthetized signals. The smallest frequency step depends on the driving clock frequency and the number of bits of the frequency register, which are set to 24 MHz and 28 bits in the current hardware. This corresponds to the above mentioned $\delta f_s = (24 \times 10^6/2^{28}) = 0.0894$ Hz.

Setting the driving clock at 24 MHz allows to get very accurate digitized waveforms in the hundreds of kilohertz region. Decreasing the clock frequency to 1 MHz, for example,

would allow to generate a $\delta f_s = 0.0037$ Hz or 3.7 mHz (comparable with the theoretical values discussed in the last row of Table II in Appendix C), but at the expense of a lower maximum attainable frequency limit. A different possibility is also using 32-bit phase and frequency registers.

Given a high enough frequency step resolution (or small δf_s), intrinsic noise in the system, such as thermomechanical and temperature fluctuations, adsorption–desorption events, defect motion, and moment exchange in gaseous atmosphere [37], [38], [39], will always be the ultimate limiting factors for detecting environmental changes. The optimal choice of δf_s should therefore be guided by the intrinsic noise of the system and the time scale of the process to be detected. As shown in Fig. 5, δf_s of the current platform is already enough to detect processes that occur in the time scale of 10 s to minutes, while can still be improved to sense subsecond phenomena.

In conclusion, as discussed in the last row of Table II, some optimizations in the present system will make possible to detect gas density variations of about 1–5 mg/m^3 using an uncoated physical resonant sensor, making it competitive to most of the commercial resistive, electrochemical and infrared absorption sensors, designed for specific detections [40]. Implementing an alternative control scheme (automatic gain control, for example) may allow to take full advantage of the maximum responsivity found far from the resonance, in regions of low-amplitude oscillation. The proposed sensing platform is general, independent on the surrounding medium, and the low-noise electronic module can still be used with a self-sensing piezoresistive cantilever, for example, or even with a resonator functionalized to a particular analyte, allowing to work with nontransparent fluids and making the platform more compact. Its sensing principles can be extended to liquid medium and to perform mass [41], viscosity [42], or viscoelasticity [43], [44] sensing. Technical solutions to stabilize the effect of cross-sensitivities to different atmospheric parameters (such as temperature, humidity, or radiation effects) must be sought [45] and implemented in real applications based on this platform.

Appendix A
Setup Details

The resonance frequency and quality factor of the microcantilever in air were measured from an external actuation with an R9 Scanning Probe Microscopy (SPM) Controller from RHK Technology. The cantilever operates in a closed cell filled with gas. Acoustic excitation of the first flexural mode is provided by a small dither piezo buried in the polyether ether ketone (PEEK) plate, in close proximity to the cantilever base. Fixation of the cantilever chip on the horizontal plane is provided by a small amount of wax or adhesive. The closed cell is connected through a polypropylene tubing system to a small PEEK container adapted with a rubber membrane, which is forced to control the pressure in the cell. A gas flow orthogonal to the cantilever beam is present in the cell when a pressure variation occurs. However, all density variations considered are slow compared to the dynamics of the PI controller embedded in the PLL, which contribute to rapidly stabilize the cantilever response.

The optomechanical unit [see Fig. 1(A)] contains a laser diode source (650-nm wavelength, 3 mW) used for the detection of the microcantilever deflection. The laser beam is deflected by a tiltable mirror and sent to a polarizing beamsplitter. The linearly polarized component follows to a quarter-wave plate, which creates a beam with circular polarization that reaches the cantilever through a focusing optics, mounted on a micrometric XYZ plate for precise adjustments. Once reflected on the cantilever, the beam passes through the quarter-wave plate and its polarization becomes linear and horizontal. It is finally deflected toward the four-quadrant detector photodiode (S4349 Hamamatsu, Japan) by the polarizing beam splitter. The tiny photocurrents are voltage-converted by a four-channels conditioning circuit (gain 10^5) placed close to the photocell to prevent any electromagnetic noise effect. The preamplified signals are fed to a custom analog algebraic board (ElbaTech Srl, Italy) that generates the deflection signal, which is finally sent to the electronics module [see Fig. 1(B)].

The electronics module, as shown in Fig. 1(B), comprises three DDDs (AD9833, Analog Devices Inc., USA), two LPs, two A/D converters, the dsPic microcontroller (dsPIC33EP512MC806, Microchip Technology Inc., USA), and the Raspberry Pi [46]. This module makes it possible to realize the control diagram shown in the orange-dotted region of Fig. 2(A). In particular, the DDDs share a common clock (24 MHz) and are thus synchronized to generate references (sine, cosine) and dither-piezo signals. The I/Q demodulators are implemented by the analog processor AD630 (Analog Devices Inc., [47]). Two fast, true-16-bit A/D converters provide the digital inputs (I and Q) to the dsPIC microcontroller, which runs direct clock-derived routines and whose firmware contains the digital control loops. The firmware serves both fast control loops and the data exchange to/from the Raspberry Pi implementing a first-in-first-out (FIFO)-based scheme.

The Raspberry Pi operates a Raspbian operating system and is directly connected to the dsPIC microcontroller by the native serial peripheral interface (SPI) and by universal asynchronous serial bus (UART) protocol for data and commands communication, respectively. It also implements high-level network communication over Ethernet with an external computer, using the ZeroMQ protocol [48]. The latter runs a GUI software, in this case a C++ application, used to send the setting parameters of the experiment (initial frequency, frequency range, imposed phase shift and dither piezo amplitude), and the desired PI gains of the control feedback. The GUI software also receives the experimental data and provides data visualization and storage.

This is a low-cost, modular and flexible architecture used for signal conditioning and data acquisition [49], [50] and designed to exploit the IoT features of Raspberry Pi mini single-board computer while adding fast real-time behavior by means of the dsPIC microcontroller.

Appendix B
Frequencies Shifts, Responsivities, and Limit of Detection

The experimental results shown in Fig. 6 are detailed in Table I. ∂f corresponds to the difference between the averaged

oscillation frequencies in the plateaus of a pressure cycle. The low and high values of frequency are calculated from averaging the frequency values from 18 to 21 s and from 22 to 25 s, respectively. Each time interval contains 3000 frequency points (sampling frequency of 1 kHz). The error associated with ∂f is determined by adding the standard deviations from the mean value of each plateau.

Appendix C
State-of-the-Art Resonant Uncoated Density Sensors

Table II compares the performance of previously reported resonant uncoated density sensors with the platform discussed in this work.

Acknowledgment

The authors would like to thank ElbaTech Srl, Italy, in the persons of Dr. Manuela Adami and Riccardo Galletti for their help with programming and testing EpsilonPi and Prof. Massimo Vassalli, University of Glasgow, Glasgow, U.K., for his contribution to the architecture and useful advices about its implementation. They would also like to thank the City Hall of Marciana, Livorno, Italy, in the Island of Elba for the hospitality and support during the testing phase of the digital circuit and platform in the laboratories of ElbaTech Srl.

References

[1] F. Schedin et al., "Detection of individual gas molecules adsorbed on graphene," *Nature Mater.*, vol. 6, pp. 652–655, Jul. 2007.

[2] L. Huang et al., "Fully printed, rapid-response sensors based on chemically modified graphene for detecting NO_2 at room temperature," *ACS Appl. Mater. Interfaces*, vol. 6, no. 10, pp. 7426–7433, May 2014.

[3] F. Gu, R. Nie, D. Han, and Z. Wang, "In_2O_3–graphene nanocomposite based gas sensor for selective detection of NO_2 at room temperature," *Sens. Actuators B, Chem.*, vol. 219, pp. 94–99, Nov. 2015.

[4] J. D. Prades et al., "Ultralow power consumption gas sensors based on self-heated individual nanowires," *Appl. Phys. Lett.*, vol. 93, no. 12, Sep. 2008, Art. no. 123110.

[5] R. Tabassum, V. S. Pavelyev, A. S. Moskalenko, K. N. Tukmakov, S. S. Islam, and P. Mishra, "A highly sensitive nitrogen dioxide gas sensor using horizontally aligned SWCNTs employing MEMS and dielectrophoresis methods," *IEEE Sensors Lett.*, vol. 2, no. 1, pp. 1–4, Mar. 2018.

[6] S. Nedelcu, K. Thodkar, and C. Hierold, "A customizable, low-power, wireless, embedded sensing platform for resistive nanoscale sensors," *Microsyst. Nanoeng.*, vol. 8, no. 1, pp. 1–11, Jan. 2022.

[7] S. Fanget et al., "Gas sensors based on gravimetric detection—A review," *Sens. Actuators B, Chem.*, vol. 160, no. 1, pp. 804–821, Dec. 2011.

[8] J. Henriksson, L. G. Villanueva, and J. Brugger, "Ultra-low power hydrogen sensing based on a palladium-coated nanomechanical beam resonator," *Nanoscale*, vol. 4, no. 16, pp. 5059–5064, 2012.

[9] Y. Hwang, H. Sohn, A. Phan, O. M. Yaghi, and R. N. Candler, "Dielectrophoresis-assembled zeolitic imidazolate framework nanoparticle-coupled resonators for highly sensitive and selective gas detection," *Nano Lett.*, vol. 13, no. 11, pp. 5271–5276, 2013.

[10] L. Aprilia et al., "CO gas-induced resonance frequency shift of ZnO-functionalized microcantilever in humid air," *J. Nanomater.*, vol. 2017, pp. 1–7, Sep. 2017.

[11] X. Fu and L. Xu, "A micro-resonant gas sensor with nanometer clearance between the pole plates," *Sensors*, vol. 18, no. 2, p. 362, Jan. 2018.

[12] N. Jaber, S. Ilyas, O. Shekhah, M. Eddaoudi, and M. I. Younis, "Simultaneous sensing of vapor concentration and temperature utilizing multimode of a MEMS resonator," in *Proc. IEEE SENSORS*, Oct. 2018, pp. 1–4.

[13] N. Jaber, S. Ilyas, O. Shekhah, M. Eddaoudi, and M. I. Younis, "Multi-mode excitation of a metal organics frameworks coated microbeam for smart gas sensing and actuation," *Sens. Actuators A, Phys.*, vol. 283, pp. 254–262, Nov. 2018.

[14] J. Xu, A. Setiono, and E. Peiner, "Piezoresistive microcantilever with SAM-modified ZnO-nanorods@silicon-nanopillars for room-temperature parts-per-billion NO_2 detection," *ACS Appl. Nano Mater.*, vol. 3, no. 7, pp. 6609–6620, 2020.

[15] G. Thomas and D. Spitzer, "3D core–shell TiO_2@MnO_2 nanorod arrays on microcantilevers for enhancing the detection sensitivity of chemical warfare agents," *ACS Appl. Mater. Interfaces*, vol. 13, no. 39, pp. 47185–47197, Oct. 2021.

[16] M. Li et al., "Nanoelectromechanical resonator arrays for ultrafast, gas-phase chromatographic chemical analysis," *Nano Lett.*, vol. 10, no. 10, pp. 3899–3903, Oct. 2010.

[17] M. T. Boudjiet et al., "Geometry optimization of uncoated silicon microcantilever-based gas density sensors," *Sens. Actuators B, Chem.*, vol. 208, pp. 600–607, Mar. 2015.

[18] L. Iglesias, M. T. Boudjiet, and I. Dufour, "Discrimination and concentration measurement of different binary gas mixtures with a simple resonator through viscosity and mass density measurements," *Sens. Actuators B, Chem.*, vol. 285, pp. 487–494, Apr. 2019.

[19] A. Loui, D. J. Sirbuly, S. Elhadj, S. K. McCall, B. R. Hart, and T. V. Ratto, "Detection and discrimination of pure gases and binary mixtures using a dual-modality microcantilever sensor," *Sens. Actuators A, Phys.*, vol. 159, pp. 58–63, Apr. 2010.

[20] A. Mahdavifar, M. Navaei, P. J. Hesketh, M. Findlay, J. R. Stetter, and G. W. Hunter, "Transient thermal response of micro-thermal conductivity detector (μTCD) for the identification of gas mixtures: An ultra-fast and low power method," *Microsyst. Nanoeng.*, vol. 1, no. 1, pp. 1–7, Oct. 2015.

[21] D. Struk, A. Shirke, A. Mahdavifar, P. J. Hesketh, and J. R. Stetter, "Investigating time-resolved response of micro thermal conductivity sensor under various modes of operation," *Sens. Actuators B, Chem.*, vol. 254, pp. 771–777, Jan. 2018.

[22] A. Z. Hajjaj, N. Jaber, N. Alcheikh, and M. I. Younis, "A resonant gas sensor based on multimode excitation of a buckled microbeam," *IEEE Sensors J.*, vol. 20, no. 4, pp. 1778–1785, Feb. 2020.

[23] Y. Xu, J.-T. Lin, B. W. Alphenaar, and R. S. Keynton, "Viscous damping of microresonators for gas composition analysis," *Appl. Phys. Lett.*, vol. 88, no. 14, Apr. 2006, Art. no. 143513.

[24] S. Tétin et al., "Modeling and performance of uncoated microcantilever-based chemical sensors," *Sens. Actuators B, Chem.*, vol. 143, no. 2, pp. 555–560, Jan. 2010.

[25] R. Rosario and R. Mutharasan, "Piezoelectric excited millimeter sized cantilever sensors for measuring gas density changes," *Sens. Actuators B, Chem.*, vol. 192, pp. 99–104, Mar. 2014.

[26] A. Badarlis, A. Pfau, and A. Kalfas, "Measurement and evaluation of the gas density and viscosity of pure gases and mixtures using a microcantilever beam," *Sensors*, vol. 15, no. 9, pp. 24318–24342, 2015.

[27] J. E. Sader, "Frequency response of cantilever beams immersed in viscous fluids with applications to the atomic force microscope," *J. Appl. Phys.*, vol. 84, no. 1, pp. 64–76, 1998.

[28] C. A. Van Eysden and J. E. Sader, "Frequency response of cantilever beams immersed in viscous fluids with applications to the atomic force microscope: Arbitrary mode order," *J. Appl. Phys.*, vol. 101, no. 4, pp. 1–11, 2007.

[29] A. Maali, C. Hurth, R. Boisgard, C. Jai, T. Cohen-Bouhacina, and J.-P. Aimé, "Hydrodynamics of oscillating atomic force microscopy cantilevers in viscous fluids," *J. Appl. Phys.*, vol. 97, no. 7, Apr. 2005, Art. no. 074907.

[30] J. Mouro, P. Paoletti, M. Sartore, M. Vassalli, and B. Tiribilli, "Photothermal self-excitation of a phase-controlled microcantilever for viscosity or viscoelasticity sensing," *Sensors*, vol. 22, no. 21, p. 8421, Nov. 2022.

[31] J. Mouro, P. Paoletti, M. Sartore, and B. Tiribilli, "Dynamical response and noise limit of a parametrically pumped microcantilever sensor in a phase-locked loop," *Sci. Rep.*, vol. 13, no. 1, Feb. 2023, doi: 10.1038/s41598-023-29420-3.

[32] J. Mouro, R. Pinto, P. Paoletti, and B. Tiribilli, "Microcantilever: Dynamical response for mass sensing and fluid characterization," *Sensors*, vol. 21, no. 1, pp. 1–35, 2021.

[33] J. Mouro, B. Tiribilli, and P. Paoletti, "Nonlinear behaviour of self-excited microcantilevers in viscous fluids," *J. Micromech. Microeng.*, vol. 27, no. 9, Sep. 2017, Art. no. 095008.

[34] A. Demir and M. S. Hanay, "Fundamental sensitivity limitations of nanomechanical resonant sensors due to thermomechanical noise," *IEEE Sensors J.*, vol. 20, no. 4, pp. 1947–1961, Feb. 2020.
[35] A. Demir, "Understanding fundamental trade-offs in nanomechanical resonant sensors," *J. Appl. Phys.*, vol. 129, no. 4, Jan. 2021, Art. no. 044503.
[36] S. Olcum, N. Cermak, S. C. Wasserman, and S. R. Manalis, "High-speed multiple-mode mass-sensing resolves dynamic nanoscale mass distributions," *Nature Commun.*, vol. 6, no. 1, pp. 1–8, May 2015.
[37] A. Cleland and M. Roukes, "Noise processes in nanomechanical resonators," *J. Appl. Phys.*, vol. 92, no. 5, pp. 2758–2769, 2002.
[38] K. L. Ekinci, Y. T. Yang, and M. L. Roukes, "Ultimate limits to inertial mass sensing based upon nanoelectromechanical systems," *J. Appl. Phys.*, vol. 95, no. 5, pp. 2682–2689, 2004.
[39] M. Sansa et al., "Frequency fluctuations in silicon nanoresonators," *Nature Nanotechnol.*, vol. 11, pp. 552–558, Feb. 2016.
[40] M. Aleixandre and M. Gerboles, "Review of small commercial sensors for indicative monitoring of ambient gas," *Chem. Eng. Trans.*, vol. 30, pp. 169–174, Sep. 2012.
[41] J. Mouro, B. Tiribilli, and P. Paoletti, "A versatile mass-sensing platform with tunable nonlinear self-excited microcantilevers," *IEEE Trans. Nanotechnol.*, vol. 17, no. 4, pp. 751–762, Jul. 2018.
[42] J. Mouro, P. Paoletti, M. Basso, and B. Tiribilli, "Measuring viscosity using the hysteresis of the non-linear response of a self-excited cantilever," *Sensors*, vol. 21, no. 16, pp. 1–13, 2021.
[43] M. Youssry, E. Lemaire, B. Caillard, A. Colin, and I. Dufour, "On-chip characterization of the viscoelasticity of complex fluids using microcantilevers," *Meas. Sci. Technol.*, vol. 23, no. 12, Dec. 2012, Art. no. 125306.
[44] E. Lemaire, B. Caillard, M. Youssry, and I. Dufour, "High-frequency viscoelastic measurements of fluids based on microcantilever sensing: New modeling and experimental issues," *Sens. Actuators A, Phys.*, vol. 201, pp. 230–240, Oct. 2013.
[45] P. Cai, X. Xiong, K. Wang, J. Wang, and X. Zou, "An improved difference temperature compensation method for MEMS resonant accelerometers," *Micromachines*, vol. 12, no. 9, pp. 1–11, 2021.
[46] *Reference Website Containing Details About the EpsilonPi Technology*. Accessed: Dec. 15, 2022. [Online]. Available: https://www.epsilonpi.it/
[47] *Datasheet of the Synchronous Demodulator Chip AD630*. Accessed: Dec. 15, 2022. [Online]. Available: https://www.analog.com/media/en/technical-documentation/data-sheets/AD630.pdf
[48] *Reference Website of the ZeroMQ Protocol for Data Exchange Over Ethernet*. Accessed: Dec. 15, 2022. [Online]. Available: https://zeromq.org/
[49] M. Sartore, M. Adami, R. Galletti, and M. Vassalli, "Flexible control for atomic-level observations," Microsolutions, Bengaluru, India, Tech. Rep., Jan. 2016.
[50] M. Sartore, M. Adami, R. Galletti, and M. Vassalli, "A quartz crystal microbalance based on a dsPIC? Digital signal controller," Microsolutions, Bengaluru, India, Tech. Rep., Apr. 2018.

João Mouro received the Ph.D. degree in technological physics from the Instituto Superior Técnico, Lisbon, Portugal, in 2015.

From 2016 to 2020, he was a Postdoctoral Fellow with the University of Liverpool, Liverpool, U.K.; the University of Bristol, Bristol, U.K.; and the Instituto de Engenharia de Sistemas e Computadores - Microsistemas e Nanotecnologias (INESC-MN) Research Center, Lisbon. He is currently with the Institute for Complex Systems, Florence, Italy, under the Marie Skłodowska-Curie Europe Union (EU) Grant. His research interests include instrumentation and microfabrication, modeling, and dynamics of MEMS devices used for sensing or digital computing.

Paolo Paoletti received the degree in automation engineering and the Ph.D. degree in nonlinear dynamics and complex systems from the University of Florence, Florence, Italy, in 2006 and 2010, respectively.

He worked as a Research Assistant with the Italian Institute for Complex Systems, Florence, in 2010, and a Postdoctoral Fellow with the School of Engineering and Applied Science, Harvard University, Cambridge, MA, USA, from 2010 to 2012. He is a Senior Lecturer in Control with the University of Liverpool, Liverpool, U.K., where he leads the Liverpool Engineering Robotics Technology (LERT) Laboratory. Since 2020, he has been the Co-Founder and the Chief Technology Officer (CTO) of the spin-off company Robotiz3d Ltd., London, U.K., which aims to introduce autonomous systems in the road maintenance industry. His research interests include nonlinear dynamics and control, with a special focus on problems that sit at the boundary between different traditional disciplines, such as biology, robotics, computer science, mathematics, and physics.

Dr. Paoletti was a recipient of the "Rising Star" Award from the U.K. Engineering and Physical Sciences Research Council in 2014.

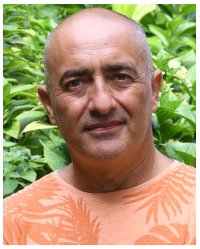

Marco Sartore was born in Sanremo, Italy, in 1964. He received the degree in electronics engineering and the Ph.D. degree in biophysics from the University of Genova, Italy, in 1989 and 1992, respectively.

He worked in the research departments of private companies leading research and development laboratories. Since 1999, he has been an Associate Member of the Board of Trustee, ElbaTech Srl, Italy, where he works as a Project Leader in Bioelectronics, working in the design and realization of electronic equipment for research experiments. Since 2021, he has been a Contract Professor with the University of Genoa, Genoa, Italy, where he also cooperates with the Department of Informatics, Bioengineering, Robotics and Systems Engineering (DIBRIS).

Bruno Tiribilli received the degree in physics from the School of Optics, University of Florence, Florence, Italy, in 1985.

In 1987, he joined an aerospace industry as a Systems Engineer. In 1990, he became a Researcher with the National Institute of Optics, Firenze, Italy; his activity concerned the development of optical instruments for scientific and industrial applications. Since 1999, his activity has been involved in the design and construction of scanning probe microscopes, mainly in Atomic Force Microscopy (AFM) and Scanning Near-field Optical Microscopy (SNOM) configuration for the study of biological systems. During this period, he was involved in several interdisciplinary studies in close collaboration with biologists, physicians, and engineers. Since 2005, he has been a Researcher with the Institute for Complex Systems, National Research Council, Florence, where he started several collaborations based on his experience on Scanning Probe Microscopy (SPM). In recent years, his activity mainly concerns the improvement of AFM techniques and the development of sensors based on cantilevers.

Open Access funding provided by 'Consiglio Nazionale delle Ricerche-CARI-CARE' within the CRUI CARE Agreement